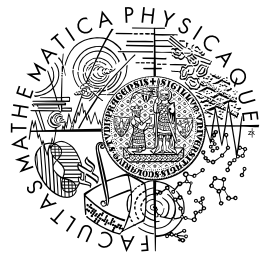

FACULTY
OF MATHEMATICS
AND PHYSICS
Charles University

BACHELOR THESIS

Matyáš Fuksa

Physical model of asteroid (130) Elektra based on adaptive optics images obtained by the VLT/SPHERE instrument

Astronomical Institute of Charles University

Supervisor of the bachelor thesis: RNDr. Josef Hanuš, Ph.D.
Study programme: Mathematical modelling

Prague 2022

I declare that I carried out this bachelor thesis independently, and only with the cited sources, literature and other professional sources. It has not been used to obtain another or the same degree.

I understand that my work relates to the rights and obligations under the Act No. 121/2000 Sb., the Copyright Act, as amended, in particular the fact that the Charles University has the right to conclude a license agreement on the use of this work as a school work pursuant to Section 60 subsection 1 of the Copyright Act.

In ..... date ....

Author's signature

Firstly I would like to thank my supervisor Dr Josef Hanuš for the supervision of this thesis and for helping me overcome my initial fear of a topic I did not know anything about. Further, my huge thanks goes to Docent Miroslav Brož, who guided me throughout the fitting process of the orbital model and helped me with any difficulties surrounding the Xitau program. Lastly, I would like to thank Dr Petr Fatka for obtaining five new lightcurves of Elektra and Master Marin Ferrais for reducing the SPHERE 2019 dataset to get the positions of the moons.

Title: Physical model of asteroid (130) Elektra based on adaptive optics images obtained by the VLT/SPHERE instrument

Author: Matyáš Fuksa

Institute: Astronomical Institute of Charles University

Supervisor: RNDr. Josef Hanuš, Ph.D., Astronomical Institute of Charles University

Abstract: Using the ADAM software package, the shape model of the asteroid (130) Elektra was reconstructed. The model is based on 60 lightcurves from the DAMIT database, 46 AO images obtained by the NIRC2 and SPHERE instruments and two occultations. The best-fit model assigns Elektra the volume of $(4.3 \pm 0.1) \times 10^6$ km^3.

After that, using the Xitau program, the orbital model of the two moons S/2014 1 and S/2003 was constructed. It is based on astrometry of the moons reduced from the 2014 and 2019 SPHERE images of Elektra. The model is a dipole non-Keplerian one, which resulted in an adjustment to the periods of the two moons to $P_1 = (1.2185 \pm 0.0004)$ d & $P_2 = (5.3015 \pm 0.0001)$ d. The main result is the more precise mass of Elektra at $(6.59 \pm 0.08) \times 10^{18}$ kg, which revises the bulk density to $\bar{\rho} = (1.533 \pm 0.066)$ g cm^{-3}.

Keywords: (130) Elektra - adaptive optics - lightcurves - shape model - orbital model

Contents

Introduction **3**

1 ADAM software package **5**
1.1 Input data types 5
1.2 How to use ADAM 7

2 Shape reconstruction of Elektra **9**
2.1 Best-fit and alternative model 11

3 Xitau program **13**
3.1 Input data 13
3.2 How to use Xitau 14

4 Orbital model **17**
4.1 Moon positions 17
4.2 Dipole non-Keplerian model 18
4.2.1 Increase of orbital periods 18
4.2.2 The resulting best-fit model 20

Conclusion **25**

Bibliography **27**

List of Figures **29**

Introduction

The asteroid (130) Elektra is located in the outer part of the main asteroid belt of our Solar System. It is remarkable for being the currently only known quadruple system, meaning that there are three much smaller bodies orbiting the central body of Elektra. This makes determining Elektra's mass and following bulk density easier and more reliable since the mass can be derived using Kepler's third law from the orbits of the satellites.

To derive the bulk density first the volume of Elektra needs to be ascertained. That is nowadays done using the All-Data Asteroid Modelling (ADAM) software package [1] (chapter 1) with which shapes of asteroids can be reconstructed from various data types. Commonly used are *lightcurves*, images from *adaptive optics* and *occultations*. Such a shape model yields the dimensions, volume, rotational pole and period of rotation of the asteroid. In this regard, Elektra was already covered several times [1, 2]. However, the ecliptic longitude of Elektra's rotational pole remains unconstrained because it is dense for the value of the ecliptic latitude.

Second, the orbital model of the system is constructed to ascertain the mass of the central body. Orbits of simulated moons are fitted on observed positions and the best-fit model is determined. Up until now, only Keplerian models of the Elektra system were constructed [3, 4, 5]. It is a simple model where the masses of the moons are neglected and the central body is taken as a singular point of mass. But, such a model does not hold up well for non-spherical asteroids, especially when it is used over a time span of several years.

This thesis aims to confirm and improve upon those previous results. In chapter 2 the shape model of Elektra is reconstructed using the aforementioned ADAM software package. The resulting best-fit model is analogous to the results from the previous works [1, 2]. Along with the best-fit model an alternative one is also listed, which is based on the revised pole of rotation derived from the orbital model.

In chapter 4 an improved orbital model of Elektra's two outermost moons is presented. It was made using the Xitau program [1] (chapter 3) which enables the construction of complex models. The presented model is a dipole non-Keplerian

[1] Made by other credited parties.

one. Dipole means that Elektra's gravitational field is generated by a dipole expansion and non-Keplerian means that the masses of the moons and their mutual influence are accounted for. Since this model considers the axis of rotation as a free parameter, one of the gained results is a revised rotational pole of Elektra. The other resulting parameters are the orbital elements of the two moons, their masses, and the mass of the central body – Elektra. This mass is then divided by the volume of the shape model to get the bulk density of Elektra.

To summarize, in the first part the reconstructed shape of Elektra is presented, which is in good agreement with the results of previous studies. In the second part, an original orbital model that is more complex, than any previously used models, is presented. The higher complexity of the model enabled deriving new and more precise orbital properties of Elektra's system.

Chapter 1

ADAM software package

All-Data Asteroid Modelling (ADAM) [6, 7] is a software package for the shape reconstruction of asteroids from various data types. These include *lightcurves*, images from *adaptive optics*, *occultations*, range-Doppler radar images and others. ADAM is free to use and available for download from the author's GitHub page [1].

The ADAM algorithm itself is based on minimizing a χ^2 function. This function is constructed in the complex plane from the square norm of the difference between the Fourier transformed initial model and Fast Fourier transformed images. In the case of other data types, special operators are used so that they also can be expressed in the complex plane. The algorithm will not be covered in any more detail since it's already explained in the author's thesis [7].

1.1 Input data types

In this section, I will briefly cover what are the usually used data types and how they are obtained. The same types are later used in the shape reconstruction of Elektra (chapter 2).

Lightcurves Are obtained by observing the brightness of an asteroid over a time period. Observed brightness depends on the asteroid's shape, surface albedo and mostly its rotation state (rotation period and direction of the spin axis) which gives the curves their periodicity as can be seen in figure 1.1. Lightcurves are, compared to the other data types, easy to obtain and for that, there is plenty of information encoded in them. This makes them an important part of any type of asteroid shape reconstruction. Lightcurves can often be sufficient to obtain a unique convex shape model. Non-convex features are seldom obtained through their usage due to uniqueness issues [7]. This is why adding additional data types is important.

[1] `https://github.com/matvii/ADAM`

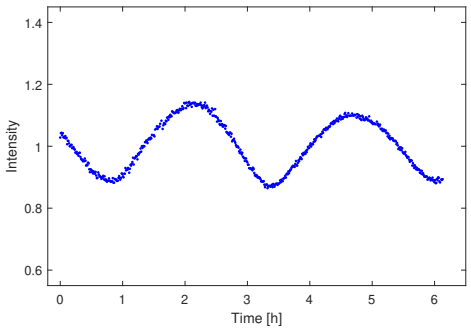

(a) Observed by G. Bolt using a telescope with a 25 cm aperture diameter at Craige, Australia on the 21st of April 2018 [8].

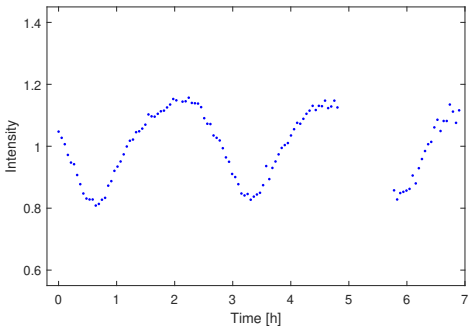

(b) Observed by P. Fatka using a telescope with a 60 cm aperture diameter [9] at Ondřejov, Czechia on the 21st of February 2021.

Figure 1.1 Two representative lightcurves of Elektra.

Adaptive optics (AO) The turbulence of the Earth's atmosphere poses a huge issue for any observations made using telescopes located on the surface of Earth, resulting in blurry images. Adaptive optics is a technology where a set of deformable mirrors controlled by a computer is able to correct for the atmospheric distortion in real-time. The resulting images are almost as sharp as those taken by telescopes located in space. [10]

In the past, AO images portrayed just an asteroid's rough shape without much surface detail visible. That changed with the installation of the Spectro-Polarimetric High contrast imager for Exoplanets REsearch (SPHERE [11]) on the Very Large Telescope (VLT) in 2014. The new images are of higher quality, the shape outline is sharper and the surface detail is more distinguishable, as can later be seen in figure 2.1. That is all crucial for the process of converging to a non-convex shape model during the algorithm.

Occultations Happen when an asteroid passes through a line of sight between an observer on Earth and a distant star, briefly occulting it. Such an event can be observed as a sudden drop in the star's brightness lasting but a few seconds. Thus, if there are several widely placed observers all watching and timing an occultation, i.e., registering their intersection with the asteroid's shadow passing over the surface of Earth. The silhouette of the asteroid can be outlined using these intersection chords, while non-detection chords put hard restrictions on the shape's boundaries.

In the algorithm, this helps to regulate the shape and prevent any wild deviations. Occultations are also useful as a final double-check. One can take the resulting shape model and manually compare it against the intersection

lines to catch any big issues with the model. This method is, specifically for Elektra, shown later in figure 2.2.

1.2 How to use ADAM

ADAM needs to be installed on a Linux-based system, compatibility with other systems is unknown. As already mentioned the software package can be downloaded from the author's GitHub page (footnote 1). On this page, there also is a list of required libraries one needs to install beforehand, but that is easily done by downloading their respective files and using the `make` command. After that, simple use of the `make all` command in the respective ADAM directory will build the whole program.

A simple command `./adam file_name.ini` will launch the program. The invoked ini file is where one links to their input and output files and edits all the config options that determine the behaviour of the algorithm.

Some example ini files are included or one can refer to the general `adam.ini` file for all the config options and their short descriptions. There also is a helpful guidebook `adam.pdf` included. It covers exactly how to select a shape representation, import data and configure it properly, and some tips on how to achieve convergence.

As a part of the software package, there also are various *MATLAB* and *Python* scripts, for visualizing input data and results, located in the `Utils` directory. The most notable one is the `adam_gui.m` script which is used to view the resulting 3D model and compare its 2D projections against the AO images and occultations (figure 2.2) of the asteroid. Another useful one is the `Display_ao_projections.m` script which captures, suggestively lit, images of the 3D model under the same viewing angles as in the AO images. Such images of the model can then be compared against the AO images of the asteroid to gauge the accuracy of the model (figure 2.4). The script can also be easily altered to capture the model from its X, Y and Z axes (figure 2.3).

Chapter 2

Shape reconstruction of Elektra

Elektra's shape reconstruction is based on 60 lightcurves, 46 AO images and two occultations. Such a huge dataset makes the resulting model grounded in reality.

Most of the lightcurves are from DAMIT [1] [12] which is a database of 3D asteroid models, lightcurves and other input data. The dataset's entries range from the year 1980 up to 2016. The five most recent lightcurves, measured in March of 2022, were obtained especially for this thesis and are not yet part of the DAMIT database. The five lightcurves were observed using the BlueEye600 robotic observatory in Ondřejov [9]. Two representative lightcurves, one from each source, were already displayed in figure 1.1.

The collection of AO images is made out of two sets. First, the 14 images captured by the Near-InfraRed Camera (NIRC2) of the Keck telescope in the years 2002-2012 and two images taken by the infrared subsystems of the SPHERE [11] instrument of the VLT in 2014 [1]. The infrared differential imager and spectrograph (IRDIS [13]) and the integral field spectrograph (IFS [14]) were used simultaneously to capture a wider array of spectra. The second set of 30 images was obtained by the Zurich IMaging POLarimeter (ZIMPOL [15]), a newer subsystem of SPHERE, in the summer of 2019 [2].

The difference between the capabilities of each instrument can be seen in figure 2.1. There is a noticeable step up in quality between the two telescopes and their instruments, but the main thing to notice is the amount of detail visible in the newest image taken by the ZIMPOL imager. ADAM can take full advantage of this, which results in a non-convex shape model with surface-level details.

Since the two occultations (figure 2.2) happened over Europe, they can be found in the results section of Asteroidal Occultation Observers in Europe [2]. The first occultation happened on the 21st of April 2018 and consisted of 47 observers from all across Europe. However, only 29 of them used the most reliable

[1] `https://astro.troja.mff.cuni.cz/projects/damit/`

[2] `http://www.euraster.net/index.html`

(a) 2005-01-15
Keck/NIRC2
pixel scale: 10 mas/pixel

(b) 2014-12-30
SPHERE/IRDIS & /IFS
pixel scale: 7.4 mas/pixel

(c) 2019-08-05
SPHERE/ZIMPOL
pixel scale: 3.6 mas/pixel

Figure 2.1 Comparison of the capabilities of the various instruments.

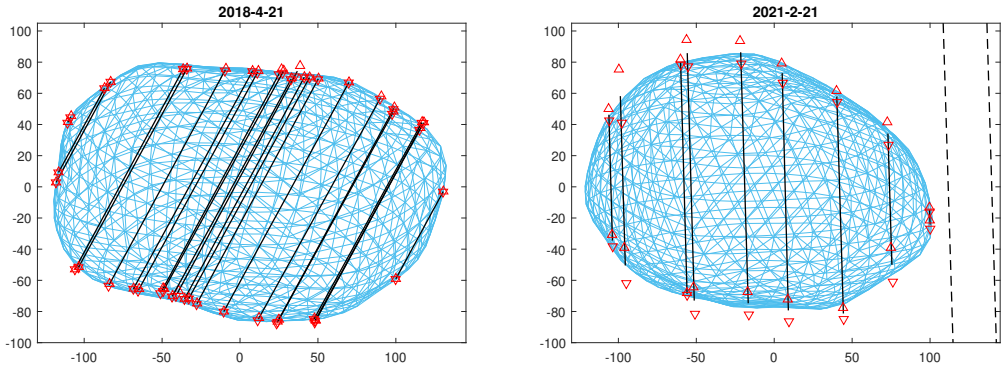

Figure 2.2 Comparison of Elektra's shape model against chords from occultation events. The *red triangles* represent timing uncertainties at the ends of each chord and the *dashed lines* are non-detection chords.

techniques, out of which the most optimal 23 chords were hand-picked. The second one happened on the 21st of February 2021, consisting of 17 observers. Eight chords were non-detection ones, but the nine remaining ones were all used. The non-detection chords weren't used, because ADAM tends to converge better without them [16].

For this modelling run, the octantoid shape representation was used. It's when the shape's surface is represented as a linear combination of spherical harmonic functions [7]. This representation is a global parametrization in other words if one were to change a parameter the whole shape would be affected [16]. The modelling was done in two phases. In the first run, the aim was to just get the rough shape of Elektra. In the second run, the resulting shape from the previous run was used as a baseline and the number of facets and spherical harmonics was doubled to dial in on the surface details.

2.1 Best-fit and alternative model

The best-fit shape model with $\chi^2 = 9.59$ is displayed from three mutually orthogonal viewing angles in figure 2.3. The model is lit up suggestively to highlight its finer surface details.

Parameters of both models are presented in table 2.1. The alternative shape model with $\chi^2 = 11.21$ is listed in table 2.1 to show that a viable solution satisfying the alternative rotational pole from section 4.2.2 exists.

In table 2.1 there are coordinates of the rotational pole, period of rotation and volume equivalent diameter which are all standard outputs of ADAM. However, the coordinates and the period need an initial guess so that they may converge or they can be fixed as is the case with the alternative pole. The extents *a,b,c* were obtained via the Overall dimensions technique [17]. The length *c* represents the extent along the spin axis, while *a* is the largest extent in the plane perpendicular to the spin axis and *b* is the largest extent in the same plane that is in addition perpendicular to *a*. The volume *V* was derived from simple formulas present in the Inertia of Any Polyhedron article [18] and is included for completion. Its use will come later in chapter 4, where the bulk density $\bar{\rho}$ of Elektra will be derived.

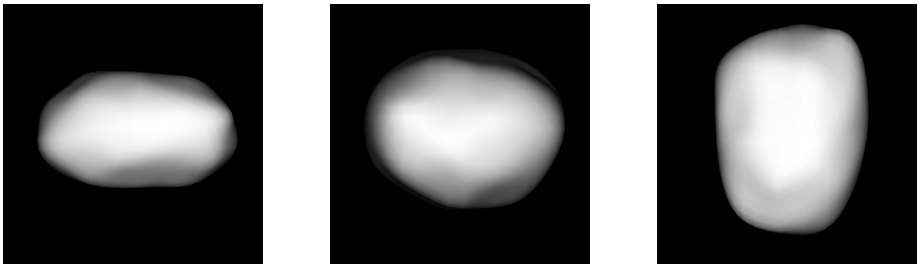

Figure 2.3 Shape model from three different points of view. The first two are *equator-on* views rotated by 90° and the third one is a *pole-on* view.

λ [deg]	β [deg]	P [h]	$a \times b \times c$ [km]	D_{eq} [km]	V [km^3]
247	−88.8	5.224663	$268 \times 203 \times 152$	201 ± 2	$(4.3 \pm 0.1) \times 10^6$
188.2	−88.1	5.224664	$273 \times 230 \times 151$	202	4.334×10^6

Table 2.1 Parameters of the models: λ & β - ecliptic coordinates of the rotational pole, P - period of rotation, *a,b,c* - extents along the main axes, D_{eq} - diameter of a volume equivalent sphere, V - volume. For the best-fit model, realistic uncertainty of the volume is given.

The low χ^2 value already indicates that the model is ideal. But, let's analyse where the final residuals come from. The first thing to check is the comparison of the shape model against the two occultations in figure 2.2. Aside from tiny inaccuracies here and there, the model corresponds completely. However, that was already known since the algorithm's readout indicated that the main portion of the value χ^2 are residuals from fitting the AO images. The figure 2.4 showcases the direct comparison of various AO images with the shape model. Here the correspondence is weaker, mainly in the two right-most images. The model just lacks such deep surface features. That can be due to the features not being as clearly visible or even present in other images or occultations, the octantoid representation or other factors.

Nevertheless, the fit is still considered good and the resulting model accurate enough. In a shape model, surface features do not have a significant impact on the volume and dimensions of the shape, which are the most important parameters of such a model.

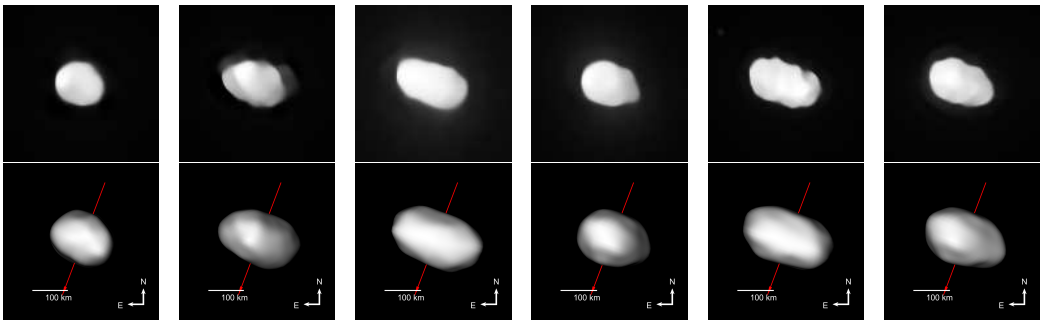

Figure 2.4 Images of Elektra (*top*) and the corresponding model (*bottom*).

Chapter 3

Xitau program

Xitau [1] is a program for simulating a full N-body model, i.e., including all mutual interactions. The program was initially developed for the construction of models of interacting multiple stellar systems [19]. However, recently it was altered to also be used for models of multiple asteroid systems [20]. Here, only the latter usage will be covered. Xitau is free to use and the newest version is available for download from the author's GitHub page [2].

On input, the program takes in orbital parameters, whereupon it simulates the trajectories of the satellites. The trajectories are calculated using the Bulirsch-Stoer numerical integrator from the SWIFT package [21]. Then the orbital model is evaluated using a χ^2 metric, which compares the observed positions of the moons with corresponding positions along the simulated trajectories, taking into account observational uncertainties.

One can then manually adjust the parameters in a search for lower χ^2 values, or there is a sub-program to minimize χ^2 as a function of the orbital parameters using the simplex algorithm [22]. However, it is recommended to use the simplex method only after manually finding orbital parameters that seem to be close to a local/global minimum of χ^2.

3.1 Input data

The not so apparent, but essential data are the trajectories of the Sun and the central body i.e. their ephemerides in the time interval of interest. Those are easily obtained from the Horizons System [3] of the Jet Propulsion Laboratory (JPL).

[1] `https://sirrah.troja.mff.cuni.cz/~mira/xitau/`

[2] `https://github.com/miroslavbroz/xitau`

[3] `https://ssd.jpl.nasa.gov/horizons/`

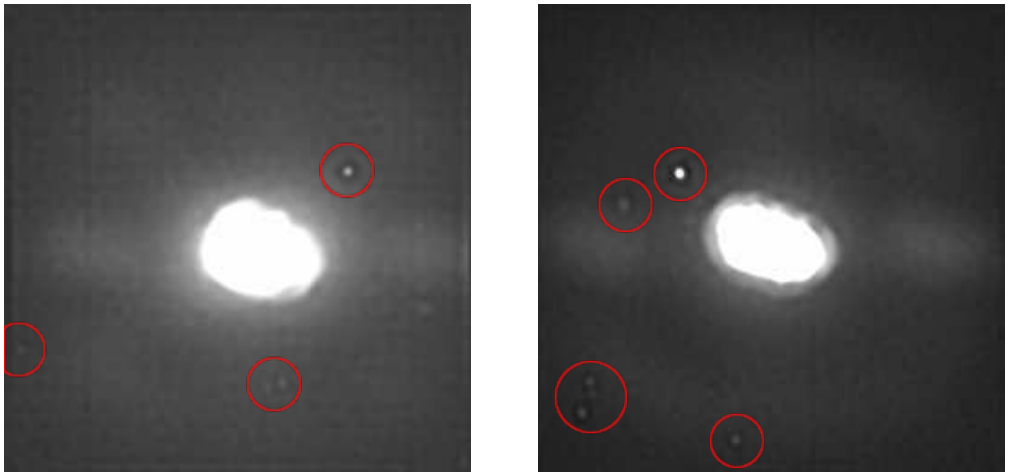

Figure 3.1 AO images of Elektra, satellite candidates are highlighted in *red*.

However, the most important type of data are the observed positions of the moons relative to the main body. Those can be obtained from the AO images of the asteroid since, after adjusting the brightness and contrast of the image, the satellites are visible in them. This can be seen in figure 3.1 where there are two images of Elektra with highlighted satellite candidates.

It may be challenging to determine which candidates are real or not from a single image. That is why several consecutive images are taken at a time, which makes the moons far easier to identify since they are the ones moving predictably. From there, the exact positions of the moons, with respect to the primary's photocentre, are determined either manually or by an algorithm.

In the case of Elektra, it even became problematic to recognize which moon is which, because of their similar orbits. However, that got resolved in the later orbital fitting stage.

3.2 How to use Xitau

Xitau needs to be installed on a Linux-based system. It can be freely downloaded from the author's GitHub page (footnote 2).

Since Xitau is written in *Fortran* the corresponding library is needed for its installation. For extra functionalities, *Gnuplot* and *Python* are required. After those are obtained a simple `make all` command will build the whole program.

As already discussed there are two main functionalities to Xitau. First is the simulation of the orbital model from fixed parameters. That is done by editing the configuration file `chi2.in` to input the parameters and observed data. Then using the `./chi2 < chi2.in > chi2.out` command which writes the command line

output of the `chi2` function into the `chi2.out` file. In which the main value of interest is the χ^2 metric of the model. In the process several other data files are also created, those are used for plotting the various results. The most notable is the plot of the orbits, which is made by a *Gnuplot* script `./chi2_SKY_uv.plt`. These can be seen in the next chapter 4. They are the main tool for visually checking the viability of the orbital model.

Second is the process of converging the orbital parameters using the simplex algorithm. The use of this algorithm is recommended only after the model has been manually arranged so that it roughly corresponds to the observed data. For this purpose there is a corresponding configuration file `simplex.in` in which one inputs the initial parameters and observed data, sets up which parameters to converge and the range of the initial perturbation of parameters. Then by the usage of a similar command `./simplex < simplex.in > simplex.out`, the output of the `simplex` function is written into the `simplex.out` file. During the algorithm, at every iteration step, the vector of parameters and the corresponding χ^2 value are noted there. The algorithm stops when a local/global minimum is reached.

Chapter 4

Orbital model

In this chapter, the orbital model of Elektra's two outermost moons, S/2003 and S/2014 1, is presented. The third moon, S/2014 2, which orbits the fastest and closest to the central body is not included in this model. Its closeness to the central body makes the fitting process technically challenging and beyond the scope of this thesis. From now on the two moons in the model shall be referred to as outer (S/2003) and inner (S/2014 1).

The orbital model evolved through several stages of increasing complexity. First, the two moons and two epochs were fitted separately using monopole Keplerian models in which the masses of the moons are neglected and the central body is taken as a singular point of mass. In the next step the two epochs were combined, but using a more accurate dipole model since the monopole one was insufficient (explained in section 4.2). Finally, the two moons were fitted into a singular dipole non-Keplerian model which takes into account their masses and in turn their mutual interaction, the effect of which is not negligible.

4.1 Moon positions

As mentioned, the orbital model is based on two datasets of moon positions. The first is a set from December of 2014, which consists of 120 positions of the inner moon and 150 positions of the outer one. Important to note is that those positions aren't independent but in reality a temporal linear fit of 40 and 50 unique measurements of positions. All the methods used in the gaining and refining of this dataset are described in the article [5] the dataset is from.

The second is a set from the Summer of 2019, consisting of 20 positions of the inner moon and 12 positions of the outer moon. This set is reduced from the same AO images as those which were used in the shape reconstruction of Elektra. It was reduced especially for this thesis.

4.2 Dipole non-Keplerian model

Due to the complicated gravitational situation around Elektra, a classical monopole Keplerian model did not hold up over such a long time span. The missing precession of orbits being an issue was mainly apparent on the trajectory of the outer moon since it did not come even close to satisfying the 2019 positions.

The source of this orbital precession is the oblateness ($J_2 \equiv -C_{20} = 0.16$) and elongation ($a/b = 1.32$) of Elektra. Thus, it was crucial to calculate the multipole expansion of Elektra's gravitational field. This was done using the same method as in article [20], the multipole coefficients are derived from the triangulated ADAM shape model.

The multipole coefficients go up to ten, but it turned out that just the dipole coefficients (table 4.1) were sufficient. That is because the dipole model was quick to converge to acceptable χ^2 values. Meanwhile, the full multipole model was much more computationally dependent and its convergence stagnated well above acceptable χ^2 values.

It was also important to include the gravitational pull of the Sun since it had a non-negligible effect on the precession of the orbits.

C_{00}	1.00000000		
C_{10}	0.00000000		
C_{11}	0.00000000	S_{11}	0.00000000
C_{20}	$-1.59109015 \times 10^{-1}$		
C_{21}	$-7.06376507 \times 10^{-5}$	S_{21}	$-1.73622001 \times 10^{-4}$
C_{22}	$-4.46764263 \times 10^{-2}$	S_{21}	$5.16249277 \times 10^{-6}$

Table 4.1 Monopole and dipole coefficients of Elektra's gravitational field derived from the shape model assuming constant density.

4.2.1 Increase of orbital periods

From the fitting of the simpler monopole model, preliminary periods of the two moons P_1 = 1.1939 d and P_2 = 5.2833 d were obtained. These are consistent with the periods already presented in the article [5]. During the transition to the dipole model, an increase of 2% and 0.3% in the periods was observed. Hence, the final periods are $P_1 = (1.2185 \pm 0.0004)$ d and $P_2 = (5.3015 \pm 0.0001)$ d. This is confirmed by figure 4.1 in which periodograms of the dipole model show the new periods occupying local minima, which from wider periodograms are known to also be global minima. Meanwhile, the old periods aren't occupying local minima and produce such high χ^2 values, that they are inconsiderable.

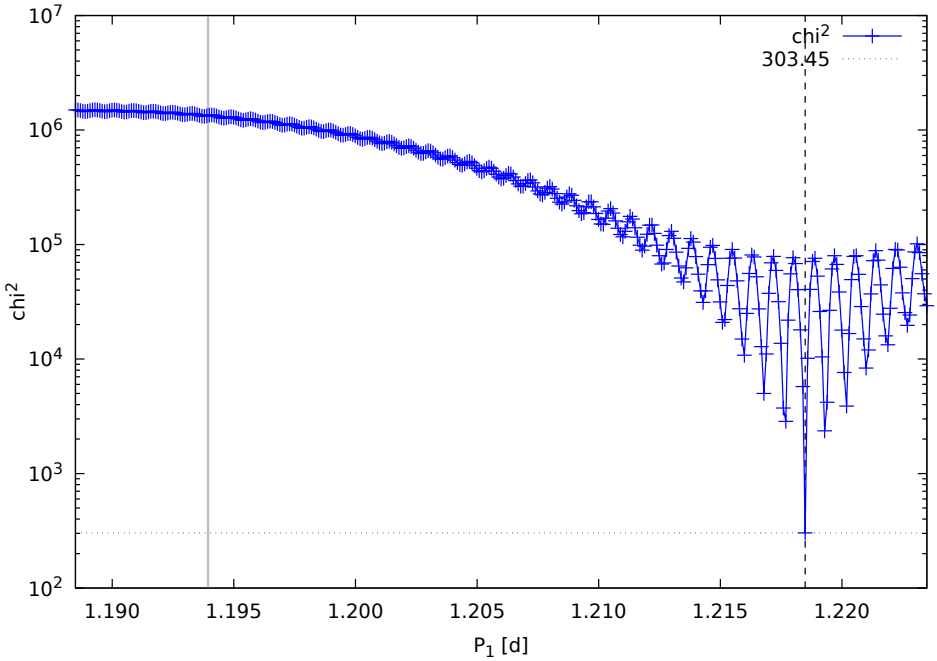

(a) Periodogram of the inner moon.

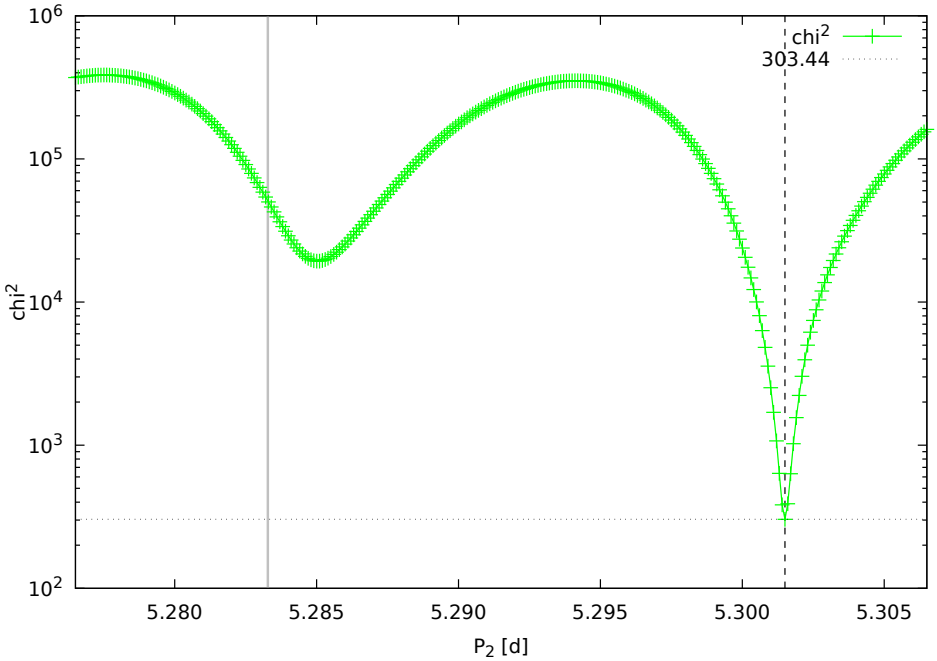

(b) Periodogram of the outer moon.

Figure 4.1 Periodograms of the dipole model. Shown are the monopole periods (*grey lines*), the dipole periods (*dashed lines*) and the minimum value of χ^2_{sky} (*dotted lines*).

4.2.2 The resulting best-fit model

In this section, the best-fit model, with $\chi^2 = \chi^2_{sky} + \chi^2_{sky2} = 349$, is presented. The terms χ^2_{sky} and χ^2_{sky2} are the goodness of fit of the absolute astrometry (i.e., bodies 2 and 3 in relation to body 1) and the goodness of fit of the relative astrometry (i.e., body 3 in relation to body 2), respectively. In figure 4.1 only χ^2_{sky} is considered.

The time integration was done 1685 days forwards and 22 days backwards in relation to T_0 = 2457021.56788 to cover both datasets. The resulting orbits are plotted in figure 4.2 or for better perspective there are separate plots covering each of the datasets in figure 4.3.

In table 4.2 parameters of the best-fit model are listed. Important to note is that the orbital elements are not constant in this advanced model and are given in relation to a particular epoch. Their oscillations over time are plotted in figure 4.4 and the results are intriguing since the peak-to-peak amplitudes of some of these elements are rather large: 3 km, 0.025 and 4° for a_1, e_1 and i_1 respectively and 1.2 km, 0.004 and 3+° for a_2, e_2 and i_2 respectively. The peak-to-peak amplitude of i_2 is given with a plus because its whole period is not even covered in the graph.

variable	unit	value	uncertainty
m_1	M_S	3.316367×10^{-12}	$\pm 0.04 \times 10^{-12}$
m_2	M_S	1×10^{-15}	$\pm 1 \times 10^{-15}$
m_3	M_S	7×10^{-16}	$\pm 7 \times 10^{-16}$
P_1	day	1.2185	±0.0004
e_1	1	0.028	±0.002
i_1	deg	180	±1.2
Ω_1	deg	275.2	±1
ϖ_1	deg	325.1	±6.3
λ_1	deg	344.5	±2.3
P_2	day	5.3015	±0.0001
e_2	1	0.125	±0.005
i_2	deg	175.3	±0.3
Ω_2	deg	134.3	±1.7
ϖ_2	deg	359.3	±4.3
λ_2	deg	293	±3.9
l_{pole}	deg	188.2	±1
b_{pole}	deg	−88.1	±1

Table 4.2 Parameters of the model. Orbital elements listed are in relation to the epoch T_0 = 2457021.56788. Uncertainties are given at 1-σ. m_1 denotes the mass of body 1 (i.e., Elektra), m_2 body 2 (first/inner moon), m_3 body 3 (second/outer moon), P_1 the orbital period of the first orbit, e_1 eccentricity, i_1 inclination, Ω_1 longitude of node, ϖ_1 longitude of pericentre, λ_1 true longitude and the same for the second orbit. l_{pole} is the ecliptic longitude of Elektra's rotational pole and b_{pole} the ecliptic latitude of it.

Now let's focus back on the parameters in table 4.2. Just to note, the uncertainties of the parameters were obtained using the Markov chain Monte Carlo (MCMC) method. The method was adapted to directly interface with the Xitau model and its script is available as part of the Xitau program. The listed uncertainties are more precise than in previous models [3, 4, 5], but that is due to the model covering a longer time interval and being more complex.

First notable parameter is the mass of Elektra, which converted to kilograms comes out to $(6.59 \pm 0.08) \times 10^{18}$ kg. This result can be combined with the volume of Elektra $(4.3 \pm 0.1) \times 10^{6}$ km^3, which was derived from the shape model in section 2.1, to obtain the bulk density $\bar{\rho} = (1.533 \pm 0.066)$ g cm^{-3}.

The other notable parameters are the ecliptic coordinates of the rotational pole of Elektra. The dipole model heavily depends on the pole, i.e., a small change in the coordinates of the pole ends up as a big change in the satellite's orbits. Thus the coordinates of the pole are determined more easily and accurately by fitting the orbits of the moons than from lightcurves via the ADAM algorithm. This alternative pole solution could be an end to the uncertainty that was up until now surrounding Elektra's pole.

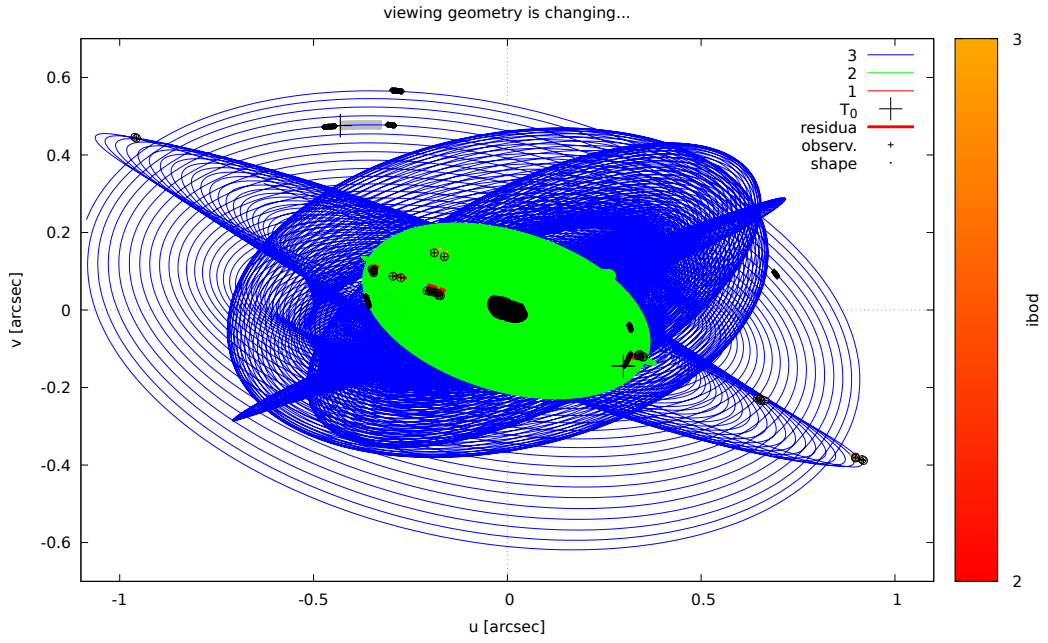

Figure 4.2 Orbits of Elektra's moons plotted in the (*u; v*) coordinates (*blue, green lines*), observed positions (*black crosses with circles*), and residuals (*red* and *orange lines* for inner and outer satellites, respectively). Elektra's shape model for one of the epochs is overplotted in *black*.

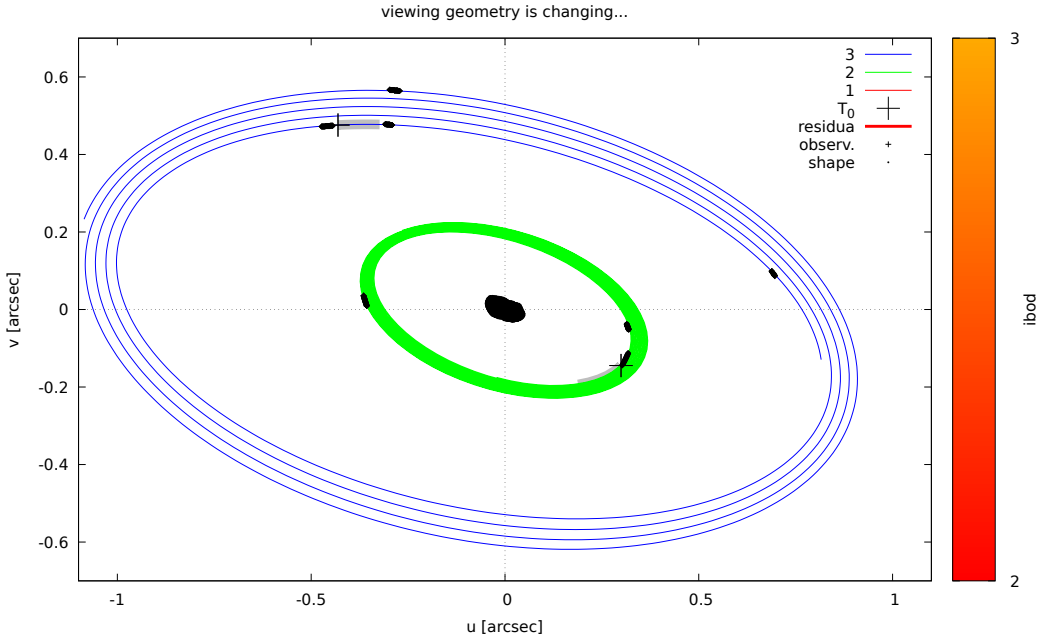

(a) Orbits of the 2014 dataset.

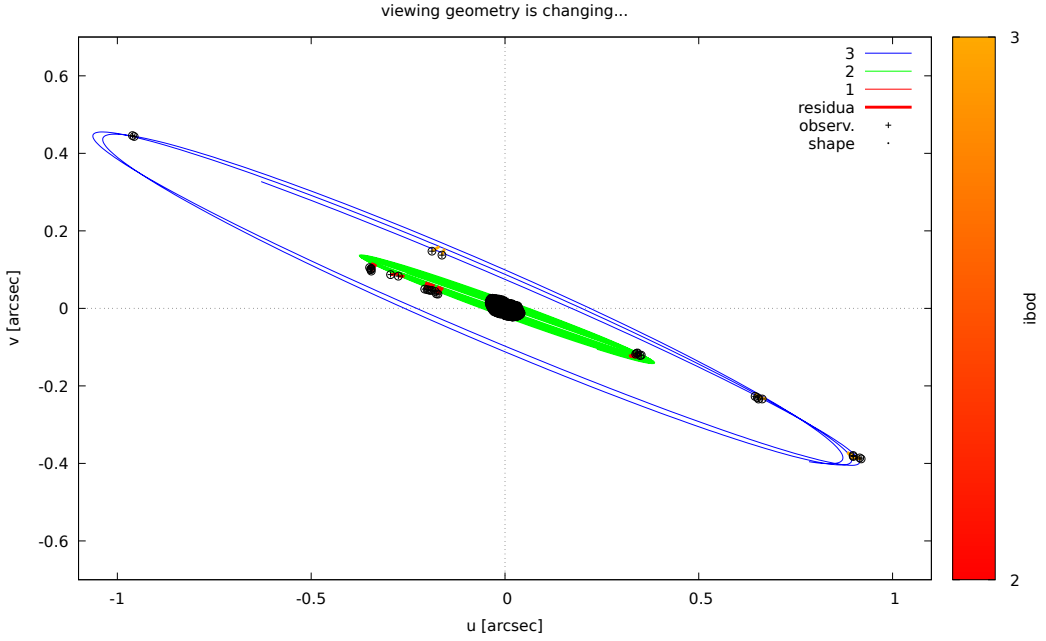

(b) Orbits of the 2019 dataset.

Figure 4.3 Same as figure 4.2, but plotted separately for each dataset.

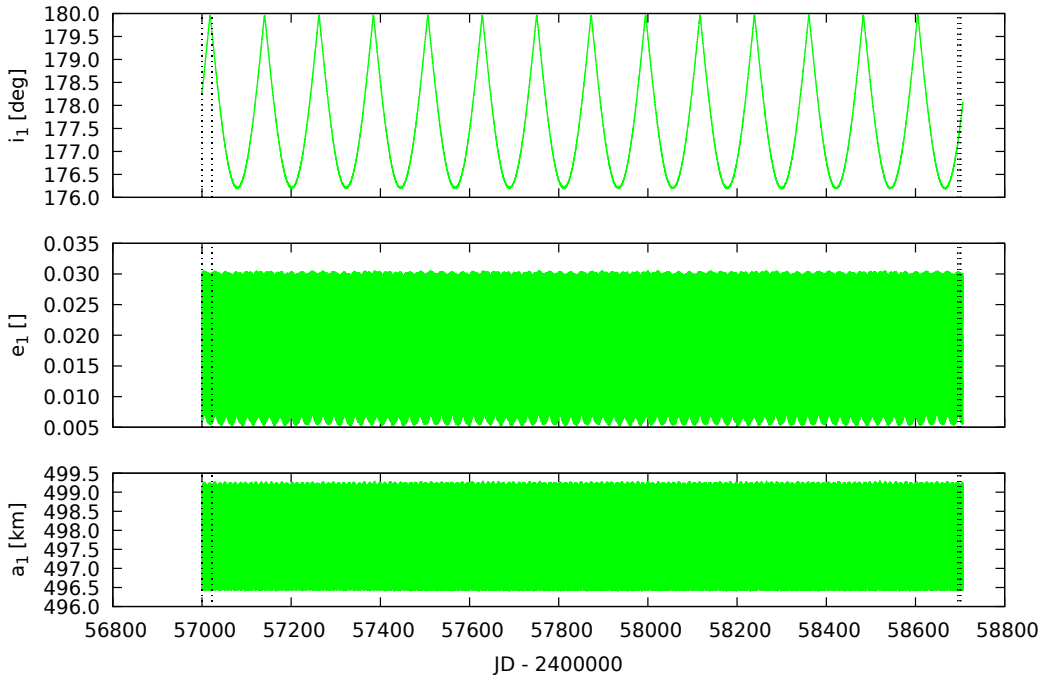

(a) Elements of the inner moon.

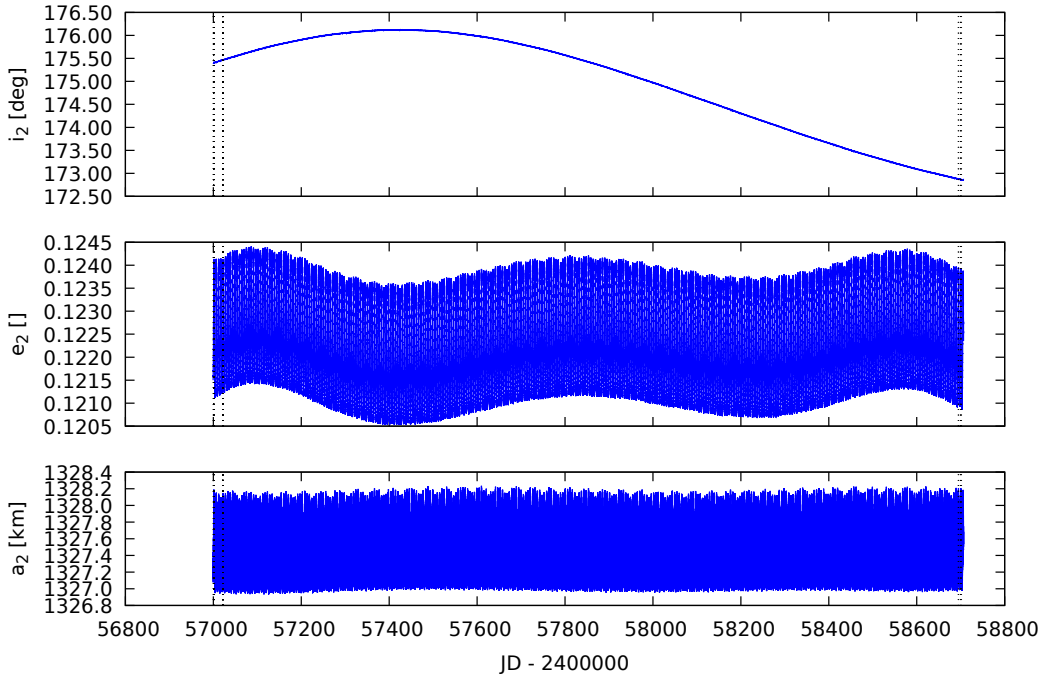

(b) Elements of the outer moon.

Figure 4.4 Evolution of the osculating elements over a time-span of 1685 d shown for the semimajor axes a_1 and a_2, eccentricities e_1 and e_2, and inclinations i_1 and i_2.

Conclusion

In the first part of the thesis, the shape model of Elektra was successfully reconstructed. The resulting best-fit model with the rotational pole $\lambda = 247^\circ$ & $\beta = -88.8^\circ$ has a volume of $(4.3 \pm 0.1) \times 10^6$ km^3 which is given with a realistic uncertainty. Additionally, an alternative model with the pole $\lambda = 188.2^\circ$ & $\beta = -88.1^\circ$ was listed to show that the pole gained from the orbital model also results in a viable solution.

The best-fit model corresponds to the parameters and uncertainties of the previous models [1, 2] of Elektra's shape, which strengthens the validity of all those results.

In the second part, the dipole non-Keplerian orbital model was constructed. From which the following parameters were gained: alternative pole and mass $(6.59 \pm 0.08) \times 10^{18}$ kg of Elektra, periods $P_1 = (1.2185 \pm 0.0004)$ d & $P_2 = (5.3015 \pm 0.0001)$ d, orbital elements and masses of the two moons. Many of these parameters, when compared with the previous Keplerian models [3, 4, 5], are altered and more accurate. Some parameters, which were previously given as constants, are now known to oscillate over time. Their evolution over time is even plotted in figure 4.4. However, as already discussed, that is all thanks to the more complex nature of the dipole model.

From the volume and mass of Elektra the asteroid's bulk density $\bar{\rho} = (1.533 \pm 0.066)$ g cm^{-3} was derived, which matches with the given densities in the previous works.

Future work

In the near future, it is planned to convert this thesis into an article for a peer-reviewed journal.

Overall this work is a step in the direction of more complex orbital models of the Elektra system, but there is still room for expansion. One could try to find a solution with an acceptable fit for the full multipole model or even add the third moon to the model for which the fitting process is quite difficult. More so, those additions will make the model even more computationally intensive.

Bibliography

[1] J. Hanuš et al. “Shape model of asteroid (130) Elektra from optical photometry and disk-resolved images from VLT/SPHERE and Nirc2/Keck”. In: *Astronomy & Astrophysics* 599 (2017), A36.

[2] P. Vernazza et al. “VLT/SPHERE imaging survey of the largest main-belt asteroids: Final results and synthesis”. In: *Astronomy & Astrophysics* 654 (2021), A56.

[3] F. Marchis et al. “Main belt binary asteroidal systems with eccentric mutual orbits”. In: *Icarus* 195.1 (2008), pp. 295–316.

[4] B. Yang et al. “Extreme ao observations of two triple asteroid systems with sphere”. In: *The Astrophysical Journal Letters* 820.2 (2016), p. L35.

[5] A. Berdeu, M. Langlois, and F. Vachier. “First observation of a quadruple asteroid”. In: (2022).

[6] M. Viikinkoski, M. Kaasalainen, and J. Ďurech. “ADAM: a general method for using various data types in asteroid reconstruction”. In: *Astronomy & Astrophysics* 576 (2015), A8.

[7] M. Viikinkoski. “Tampere University of Technology”. PhD thesis. PhD thesis, 2016.

[8] J. Ďurech et al. “Physical models of ten asteroids from an observers’ collaboration network”. In: *Astronomy and Astrophysics* 465.1 (2006), pp. 331–337.

[9] J. Ďurech et al. “Shape models of asteroids based on lightcurve observations with BlueEye600 robotic observatory”. In: *Icarus* 304 (2018), pp. 101–109.

[10] ESO. *ESO Adaptive Optics*. 1991. URL: `https://www.eso.org/public/teles-instr/technology/adaptive_optics/` (visited on 05/31/2022).

[11] J.-L. Beuzit et al. “SPHERE: the exoplanet imager for the Very Large Telescope”. In: *Astronomy & Astrophysics* 631 (2019), A155.

[12] J. Ďurech, V. Sidorin, and M. Kaasalainen. “DAMIT: a database of asteroid models”. In: *Astronomy & Astrophysics* 513 (2010), A46.

[13] K. Dohlen et al. “The infra-red dual imaging and spectrograph for SPHERE: design and performance”. In: *Ground-based and Airborne Instrumentation for Astronomy II*. Vol. 7014. SPIE. 2008, pp. 1266–1275.

[14] R. U. Claudi et al. “SPHERE IFS: the spectro differential imager of the VLT for exoplanets search”. In: *Ground-based and Airborne Instrumentation for Astronomy II*. Vol. 7014. SPIE. 2008, pp. 1188–1198.

[15] H. M. Schmid et al. “SPHERE/ZIMPOL high resolution polarimetric imager-I. System overview, PSF parameters, coronagraphy, and polarimetry”. In: *Astronomy & Astrophysics* 619 (2018), A9.

[16] M. Viikinkoski. *ADAM software: Some tips on usage*.

[17] J. Torppa et al. “Asteroid shape and spin statistics from convex models”. In: *Icarus* 198.1 (2008), pp. 91–107.

[18] A. R. Dobrovolskis. “Inertia of any polyhedron”. In: *Icarus* 124.2 (1996), pp. 698–704.

[19] M. Brož. “An Advanced N-body Model for Interacting Multiple Stellar Systems”. In: *The Astrophysical Journal Supplement Series* 230.2 (2017), p. 19.

[20] M. Brož et al. “An advanced multipole model for (216) Kleopatra triple system”. In: *Astronomy & Astrophysics* 653 (2021), A56.

[21] H. F. Levison and M. J. Duncan. “SWIFT: A solar system integration software package”. In: *Astrophysics Source Code Library* (2013), ascl–1303.

[22] J. A. Nelder and R. Mead. “A simplex method for function minimization”. In: *The computer journal* 7.4 (1965), pp. 308–313.

List of Figures

1.1 Two representative lightcurves of Elektra. 6

2.1 Comparison of the capabilities of the various instruments. . . . 10
2.2 Comparison of Elektra's shape model against chords from occultation events. The *red triangles* represent timing uncertainties at the ends of each chord and the *dashed lines* are non-detection chords. 10
2.3 Shape model from three different points of view. The first two are *equator-on* views rotated by 90° and the third one is a *pole-on* view. 11
2.4 Images of Elektra (*top*) and the corresponding model (*bottom*). . 12

3.1 AO images of Elektra, satellite candidates are highlighted in *red.* 14

4.1 Periodograms of the dipole model. Shown are the monopole periods (*grey lines*), the dipole periods (*dashed lines*) and the minimum value of χ^2_{sky} (*dotted lines*). 19
4.2 Orbits of Elektra's moons plotted in the (*u; v*) coordinates (*blue, green lines*), observed positions (*black crosses with circles*), and residuals (*red* and *orange lines* for inner and outer satellites, respectively). Elektra's shape model for one of the epochs is overplotted in *black*. 21
4.3 Same as figure 4.2, but plotted separately for each dataset. . . . 22
4.4 Evolution of the osculating elements over a time-span of 1685 d shown for the semimajor axes a_1 and a_2, eccentricities e_1 and e_2, and inclinations i_1 and i_2. 23